Micro-pressure wave radiation from tunnel portals in deep cuttings

Wang, Honglin; Vardy, Alan E.; Bi, Haiquan

Published in:
Proceedings of the Institution of Mechanical Engineers, Part F: Journal of Rail and Rapid Transit

DOI:
10.1177/09544097221099393

Publication date:
2022

Document Version
Peer reviewed version

Wang, H, Vardy, AE & Bi, H 2022, 'Micro-pressure wave radiation from tunnel portals in deep cuttings', Proceedings of the Institution of Mechanical Engineers, Part F: Journal of Rail and Rapid Transit. https://doi.org/10.1177/09544097221099393

Micro-pressure wave radiation from tunnel portals in deep cuttings

Honglin Wang[1*], Alan E Vardy[2], Haiquan Bi[1]

1 School of Mechanical Engineering, Southwest Jiaotong University, China

2 School of Science and Engineering, University of Dundee, UK

*Corresponding author:
Honglin WANG

Address for correspondence:
School of Mechanical Engineering, Southwest Jiaotong University, China
E: honglinwang305@hotmail.com

ABSTRACT

The reflection and radiation of steep-fronted wavefronts at a tunnel exit to a deep cutting is studied and contrasted with the more usual case of radiation from over-ground portals. A well-known difference between radiation in odd and even dimensions is shown to have a significant influence on reflected wavefronts, notably causing increased distortion that complicates analyses, but that can have practical advantages when rapid changes are undesirable. Likewise, micro-pressure waves radiating from the portal into a cutting are shown to exhibit strong dispersion that does not occur in the corresponding radiation into an open terrain. In the latter case, formulae that represent the behaviour of monopoles and dipoles are commonly used to estimate conditions beyond tunnel portals, but no such simple formula exists (or is even possible) for cylindrical radiation that is characteristic of MPWs in cuttings. An important outcome of the paper is the development of an approximate relationship that predicts the maximum amplitudes of these MPWs with an accuracy that should be acceptable in engineering design, at least for initial purposes. The formula shows that peak pressure amplitudes decay much more slowly than those from an overground portal, namely varying approximately as $r^{-0.5}$ compared with r^{-1}, where r denotes the distance from the portal.

Keywords: Micro-pressure waves; railway cuttings; tunnels; flanged portals; 2-D radiation

Nomenclature

1-D	one dimensional	*MPW*	micro-pressure wave
2-D	two dimensional	P	absolute pressure
3-D	three dimensional	P_{amb}	ambient absolute pressure
A	cross-sectional area of tunnel	p	acoustic/gauge pressure (P-P_{amb})
c	speed of sound	r	radius or distance from effective source
D	width of (square section) tunnel	t	time coordinate
D_{eff}	effective diameter of tunnel	t^*	retarded time
H	flow width normal to 2-D plane of propagation	x,y,z	spatial coordinates (see Fig.3)
L	length of tunnel	x'	distance (outside tunnel) from exit plane

ℓ	end correction coefficient	***Greek characters***	
$\dot{m}$	mass flow rate	θ	angle subtended to tunnel axis, radians
$\dot{m}_z$	mass flow rate per unit width (2-D case)	Ω	solid angle, steradians

1 INTRODUCTION

The radiation of micro-pressure waves (MPWs) into environments outside railway tunnels as a consequence of pressure wave activity inside the tunnels is well understood, at least generically. In extreme cases, strong emissions can occur in the audible frequency range.[1-2] Likewise, radiation in the sub-audible range can cause unacceptable vibrations of doors and windows in buildings.[3] Almost all publications on this topic deal with tunnels emerging above ground level (Fig.1a). In this case, the radiation occurs into a geometrical space that is unbounded in any of the three principal directions (*x*,*y*,*z*). However, it is increasingly common for new tunnels to emerge into cuttings (Fig.1b), sometimes quite deep ones. In this case, the radiation occurs into a geometrical space that greatly constrains it in the *z*-direction normal to the plane of the figure. The radiated waves do not escape this constraint until after they have reached ground level (G.L.). In both geometries, the radiation beyond moderate distances from the portal (i.e. in the so-called far-field) approximates quite well to the purely radial radiation illustrated in Fig.1c. For the overground case, this radiation is approximately spherical whereas, within a cutting, it is closer to cylindrical. Indeed, the particular cutting considered in detail herein has vertical sides (as is typical beyond cut-and-cover tunnels) and is the same width as the tunnel. With this geometry, the radiation is truly two-dimensional (*x*,*y*) – for the same reason that wave propagation along the tunnel itself occurs in an effectively one-dimensional manner (*x*) that justifies neglecting lateral (*y*,*z*) variations in pressure over the tunnel cross-section.

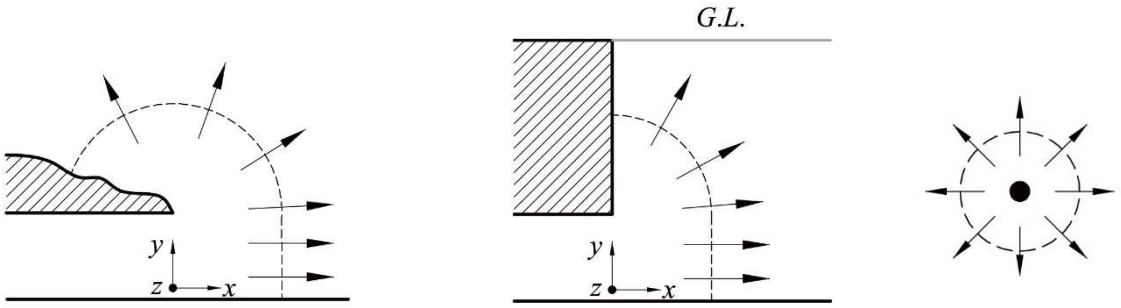

(a) Overground portal (3-D) (b) Deep cutting (2-D) (c) Point source

Fig.1. Radiation from tunnel exits and a point source

Following a preliminary investigation of this phenomenon[4], the authors reported that MPWs in cuttings exhibit large qualitative differences from those from overground MPWs, but they were unable to provide convincing explanations for this. Several possible contributions to the differences were hypothesized, one of which was that it might arise from fundamental differences between radiation in two (*x*,*y*) and three (*x*,*y*,*z*) dimensions[5]. The primary purpose of the present paper is to assess this possibility and to show that it does indeed seem to be a likely cause. Having first demonstrated this, the paper moves on to the development of an equation that is shown to be a close predictor of the maximum amplitudes of MPWs in deep cuttings. However, it is also

shown that, unlike the corresponding equation for radiation from overground portals, the new equation must not be used to represent the shape of complete pulses. This is interpreted as a further demonstration of the big differences between radiation in 2-D and 3-D geometries.

The initial desire to study this topic was triggered by enquiries from tunnel designers. The authors felt unable to advise reliably on these, but realised that that they posed intriguing academic questions. Following standard research practice, after spending time developing some initial ideas, the authors began to search the literature for relevant prior publications. The result was unexpected. Not only were no examples found of the specific topic, but also no publications at all on practical applications in the time domain were found. This does not, of course, mean that no such studies exist, but it is a strong indicator that any that do exist are rare. Analyses applicable to cylindrically radial radiation from a line source do exist, but these mostly consist of analytical methodologies in the context of periodic waves and involve either high-level mathematics or tedious summations [6-10]. They cannot readily be adapted to studying the radiation of sudden wavefronts from tunnel portals. Usually, cylindrical radiation is presented more briefly than spherical radiation. The authors take this opportunity to invite readers to alert them to any work that has been missed.

1.1 Terminology

In the remainder of the paper, attention is sometimes focussed dominantly on the practical application and is sometimes focussed on the fundamental nature of wave propagation. In the former case, the distinction is between an overground portal and a portal in a deep cutting that, for the purposes of this paper, is assumed to be the same width as the tunnel. However, when discussing the wave propagation itself, it is more natural to use terminology that denotes generic behaviour. In this context, therefore, the wave propagation is usually characterised as 2-D (i.e. x,y) or 3-D (i.e. x,y,z). In special cases, it is idealised even further as 'cylindrical' and 'spherical' in the sense represented in Fig-1c.

1.2 Wavefront reflection and pulse generation

To set the scene, the mechanism by which internal waves cause MPWs is now summarised. Figure 2a depicts an abrupt, step wavefront representing, say, a train nose-entry wavefront after it has steepened almost into a shock during propagation along a tunnel. As the wavefront approaches the exit portal, the pressure at any axial location ahead of or behind it is almost uniform over the tunnel cross-section. Ahead of the wavefront, the pressure is atmospheric whereas that behind it is greater than atmospheric. On arrival at the exit (Fig.2b), the region behind the uppermost tip of the wavefront begins to be influenced by the external (atmospheric) pressure and in the next few moments, local radiation propagates over the cross-section. However, this takes time – approximately D/c, where D is the tunnel height and c is the speed of sound – during which the lower parts of the wavefront continue exactly as before, as indicated schematically in Fig.2c. This has the twin effect of (i) delaying and distorting the reflection back along the tunnel and (ii) creating a short period of strongly unsteady flow into the external domain. It causes a pulse-like pressure wave to radiate outwards from the portal – approximately spherically in the overground case, but cylindrically in a deep cutting. The main thrust of the

paper is on the radiated pulse, but consequences for reflected wavefront inside the tunnel are also highlighted.

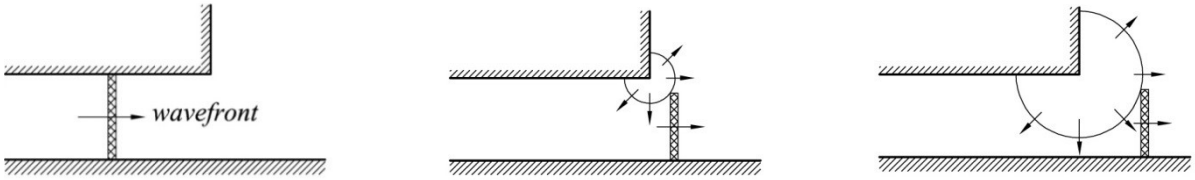

(a) incident wavefront (b) shortly afterwards (c) a little later still

Fig.2. Radiation of a pressure pulse from a tunnel exit

2 METHODOLOGY

Figure 3 shows the calculation domains used for the simulations. Advantage is taken of the use of symmetry to greatly reduce the required CPU resources. The flanged portal is a distance *L = 100 m* from an upstream location *x* = 0 at which the pressure is prescribed to increase rapidly, representing an approaching wavefront. The *y*-axis is vertically upwards and the *x,z* plane at *y* = 0 is modelled as a plane of symmetry that is chosen to coincide with the base of the tunnel (i.e. track level). That is, the tunnel is of width *D = 8 m* and height *½D*. Beyond the exit, the domain extends a distance *L* in each of the *x* and *y* directions. For the above-ground (3-D) geometry, it also extends a distance *L* in the z direction, but for the cutting (2-D) geometry, the domain is the same width as the tunnel in the *z* direction. In both cases, the plane *z* = 0 is modelled as a plane of symmetry that is chosen to coincide with the centre-line of the tunnel. Thus, although the tunnel itself is of width *D*, the calculation domain is only half this width.

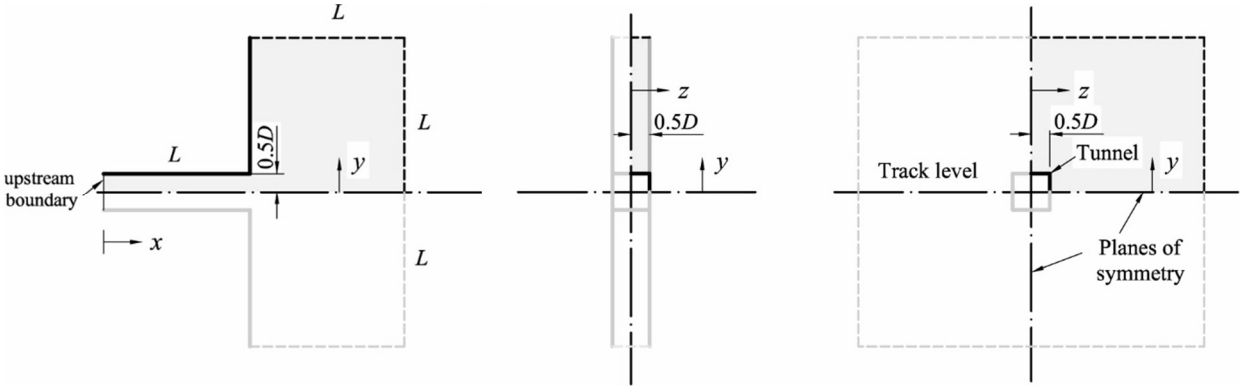

(a) *x-y* plane (2-D & 3-D) (b) *y-z* plane, 2-D (c) *y-z* plane, 3-D

Fig.3. Calculation domains and definition of axes (*x* = axial; *y* = vertical; *z* = lateral)
Calculations are required only within y ≥ 0 and z ≥ 0 because the planes at y = 0 and z = 0 are planes of symmetry

The simulations are undertaken numerically, using the commercially-available software ANSYS FLUENT 15.0[11] with the following options: density-based solver, Roe-FDS Flux Scheme, third-order MUSCL for spatial discretisation and second-order implicit time stepping for temporal

discretisation. User-defined functions are used to determine the maximum pressure at each point in the calculation domain and the instant at which it occurs. Formal validation of the suitability of the chosen numerical grid is presented in an Appendix.

All of the following simulations have been undertaken using the 3-D version of the code even though this is not strictly necessary for 2-D cases. This eliminates any risk of comparisons between predictions being influenced by differences between 2-D and 3-D solvers, thereby reducing the reliability of comparisons of the influences of the two geometries. Also, inviscid conditions are assumed. This simplification, which aids clarity, introduces negligible error because turbulence-related disturbances can propagate only tiny distances during the short time scales under investigation. The authors have illustrated the validity of this statement in publications of other work on wave propagation[12]

2.1 Governing equations

All simulations have been undertaken using the 3D Euler equations throughout the whole of the flow-field. The phenomena under investigation occur in such short timescales that the influence of viscous effects will inevitably be negligible in comparison with inertial effects. In the absence of heat sources, the governing equations are

$$\mathbf{U}_t + \mathbf{F}_x + \mathbf{G}_y + \mathbf{H}_z = 0 \tag{1}$$

in which

$$\mathbf{U} = \begin{bmatrix} \rho \\ \rho u \\ \rho v \\ \rho w \\ \rho E \end{bmatrix}, \quad \mathbf{F} = \begin{bmatrix} \rho u \\ \rho u^2 + P \\ \rho uv \\ \rho uw \\ \rho uH \end{bmatrix}, \quad \mathbf{G} = \begin{bmatrix} \rho v \\ \rho vu \\ \rho v^2 + P \\ \rho vw \\ \rho vH \end{bmatrix}, \quad \mathbf{H} = \begin{bmatrix} \rho w \\ \rho wu \\ \rho wv \\ \rho w^2 + P \\ \rho wH \end{bmatrix} \tag{2}$$

where x , y ,z are spatial coordinates, t is the time coordinate, u, v, w are the components of the velocity $\boldsymbol{V}$ in the x , y and z directions, and ρ and P are the air density and absolute pressure. The specific total energy E and the specific total enthalpy H are

$$E = \frac{1}{\gamma - 1}\frac{P}{\rho} + \frac{1}{2}\mathbf{V}^2 \qquad H = E + \frac{P}{\rho} \tag{3}$$

in which γ denotes the ratio of the principal specific heat capacities of the air.

The equations are closed by regarding the air as a perfect gas satisfying the equation of state:

$$P = \rho R_{gas} T \tag{4}$$

where R_{gas} is the gas constant for air and T is the absolute temperature.

A slip boundary condition is used on all solid surfaces and null-reflection conditions are prescribed at the outer boundaries of the external domains - although these are chosen sufficiently far from

the portal to have no influence whatsoever on the presented results. Initially, ambient conditions exist everywhere. The pressure at the upstream end of the tunnel then increases in a prescribed manner to generate the incident wavefront.

The accuracy of the simulations has been assessed in academic detail. In particular, it is shown in an Appendix that the predictions are effectively independent of grid size. Also, Wang et al [12] have shown that wavefront steepening is modelled with good accuracy and it is shown below that predictions of MPWs in the overground case coincide closely with analytical expectations.

2.2 Incident wavefront

Figure 3 shows a typical prescribed pressure history at the upstream boundary. The *rate of change* of pressure increases linearly to a maximum and then decreases to zero at an equal and opposite rate. The resulting shape of the wavefront is broadly indicative of nose-entry wavefronts – see, for example, Figs. 10 & 17 in Miyachi et al[2]. In the particular example shown in Fig.4, the wavefront amplitude is 2 kPa and its initial maximum steepness and length are 40 kPa/s and 34 m. Predictions are also presented below for wavefronts with the same pressure amplitude, but with maximum steepnesses of 80, 20 and 10 kPa/s respectively.

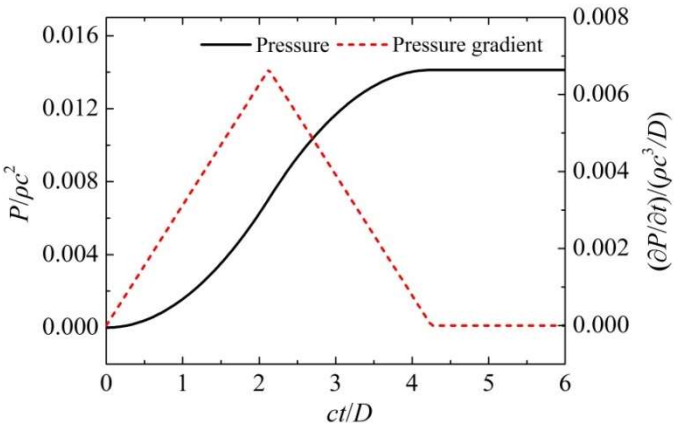

Fig.4**. 40 kPa/s incident wavefront**

The prescribed pressure is imposed at the upstream boundary which, in the simulations, is a distance L = 100 m (i.e. 12.5D) upstream of the portal. As the resulting wavefront propagates downstream, it gradually shortens under the influence of inertial steepening. The toe of the wavefront – i.e. its leading tip – travels at the ambient speed of sound, but the rear of the wavefront travels at a greater speed, partly because the increased pressure behind the wavefront causes a small increase Δc in the speed of sound, but mostly because of the increase ΔU in air velocity that the wavefront induces. The overall difference in wavespeed between the toe and rear of the wavefront is $\Delta(U + c)$ and for the chosen wavefront amplitude of 2 kPa, this is approximately equal to 6 m/s. In the absence of friction, this difference in propagation speeds causes the wavefront to shorten – and hence to steepen in a manner that is loosely analogous to that observed in surface waves approaching a beach. In the tunnel, the difference in speed causes a reduction of slightly more than 0.2D in the length of the wavefront as it travels 100 m from the upstream boundary to the exit portal. All of these values (distances and speeds) are independent

of the initial length of the wavefront so each necessarily shortens by the same amount. However, the *proportional* influence of the shortening is greater for initially short wavefronts than for longer ones, so the consequences are more important for the steeper wavefronts.

2.3 Non-dimensional parameters

Although the simulations have been performed using dimensional values, all results are presented and interpreted in a non-dimensional manner. This has an important advantage in the development of a new generic expression in Section 5. The chosen length scale is D (see Fig.3), the time scale is D/c, where c is the ambient speed of sound and the mass scale is ρD^3, where ρ is the density of the ambient air. The pressure p scales with ρc^2, the mass flow rate $\dot{m}$ scales with $\rho c D^2$ and rates of change of mass flow rate scale with $\rho c^2 D$. In the 2-D simulations, the relevant mass flow rate parameter, denoted $\dot{m}_z$, is the mass flow rate per unit width normal to the plane in which waves are propagating. Its scale is $\rho c D$ and its rate of change scales with ρc^2. For record purposes, in the particular simulations on which subsequent figures are based, D = 8m, L = 100 m, c = 340 m/s and ρ = 1.225 kg/s.

3 REFLECTED WAVEFRONTS

In addition to causing the radiation of a pulse, the process illustrated in Fig.2 causes distortion and delay of reflections back along the tunnel. This can have a (small) influence on phenomena of importance on trains – e.g. passenger aural comfort[13] and forces on train bodies[14]. Therefore, it is useful to assess it in its own right as well as for providing information of relevance to the interpretation of predicted radiated pulses.

Figure 5 shows instantaneous pressure distributions along the tunnel at representative instants before and after the reflection (NB: x/D = 12.5 corresponds to $x = L$). In each box, an incident wavefront (continuous line) travelling from left-to-right is shown at the instant when its mid-point is at $x = L/2$. The reflected wavefronts (broken lines) are shown at an instant L/c later. By inspection, the shapes of the incident and reflected wavefronts are very different, whereas they would be identical if the reflection process at the exit occurred instantaneously (as is usually assumed in 1-D calculations, for instance). Instead, strong delays are apparent, and these are much greater in later stages of the reflection than in the early stages. It is shown below that the delays can also be observed in the resulting pressure fields beyond the portals.

It can be seen in the figure that the absolute values of the delays for the various wavefronts do not differ greatly from one another. They do differ, but not by anywhere near as much as the differences in length of the wavefronts. This demonstrates that the effect is dominated primarily by conditions in the exit region, not by properties of the wavefronts themselves.

The dotted grey lines in the figures are provided for information only. They illustrate what would happen if the reflection process were instantaneous, but occurred a small distance outside the portal. This seemingly arbitrary approximation – designated an end-correction – can be highly effective in studies of periodic waves[15-16]. By inspection, however, it is of little value in any attempt to explain the wavefront reflections herein, and this is predictable because the wavefronts differ greatly from single-frequency periodic waves.

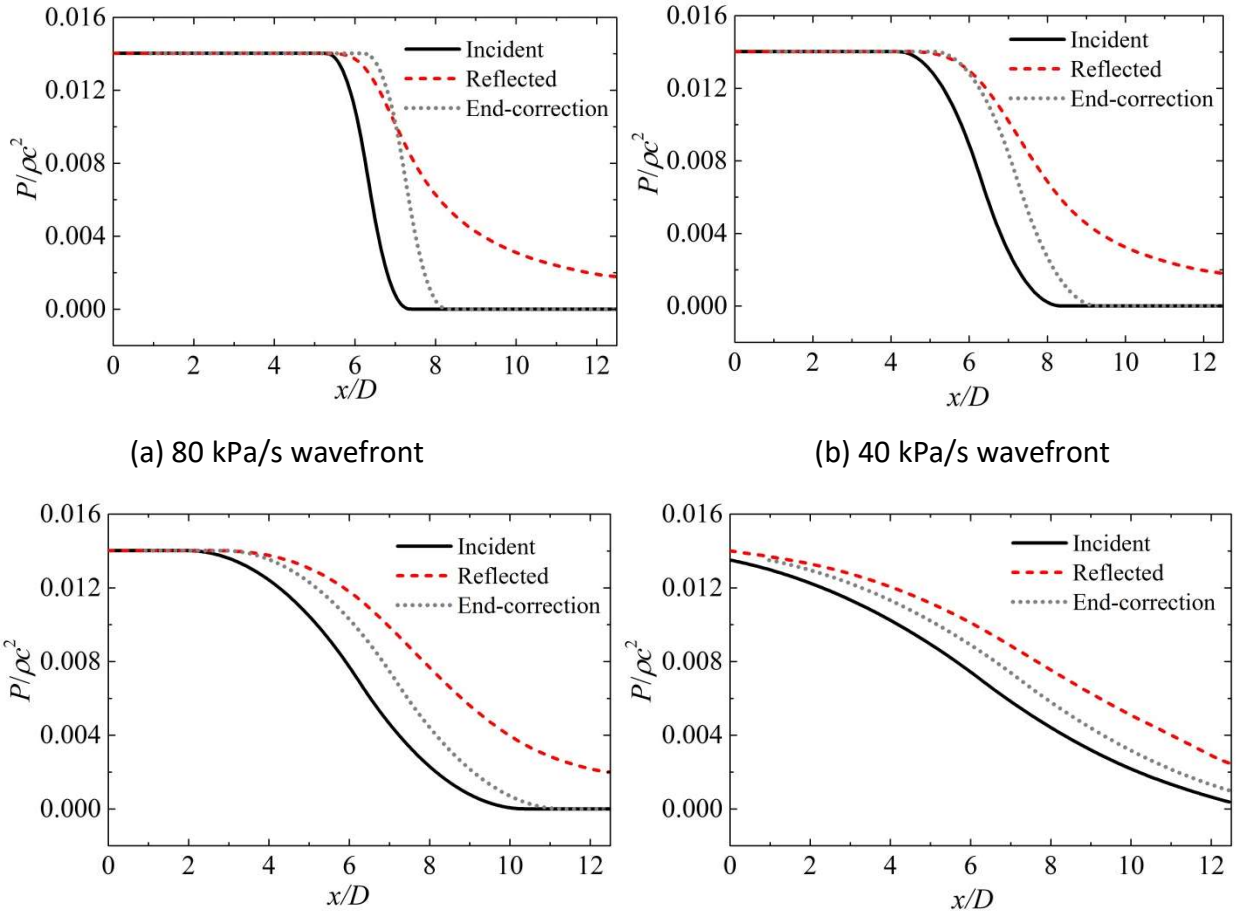

(a) 80 kPa/s wavefront

(b) 40 kPa/s wavefront

(c) 20 kPa/s wavefront

(d) 10 kPa/s wavefront

Fig.5. Instantaneous pressure distributions along the tunnel (2-D external geometry)

3.1 Flow rate through the exit portal

The upper row in Fig.6 shows predicted flow rate histories through the portal in the cutting (2-D), with corresponding predictions for an overground portal also shown for comparison purposes (3-D). In each case, the flow rates increase smoothly from zero and become asymptotic to a maximum value that is approximately equal to twice the rate induced by the incident wavefront during propagation towards the exit. The strong delays in the 2-D case have an important influence on the resulting pulses radiated into the external environment. However, the latter depend dominantly on *rates of change* of flow through the portal, not on *absolute* flow rates. These rates are shown in the lower row of the figure. The ranges of the vertical axes are chosen in proportion to the wavefront steepnesses, thereby providing a simple visual demonstration that the maximum rate of change also scales approximately with the wavefront steepness.

For completeness, it should be noted that the vertical axes in the figure are applicable to *absolute* mass flow rates. In the case of 2-D flows, the stated non-dimensionalisation implies an

assumption that the domain has a finite width D in the z-direction. In Section 5 below, analytical expressions utilise a more general presentation based on flow rate per unit width.

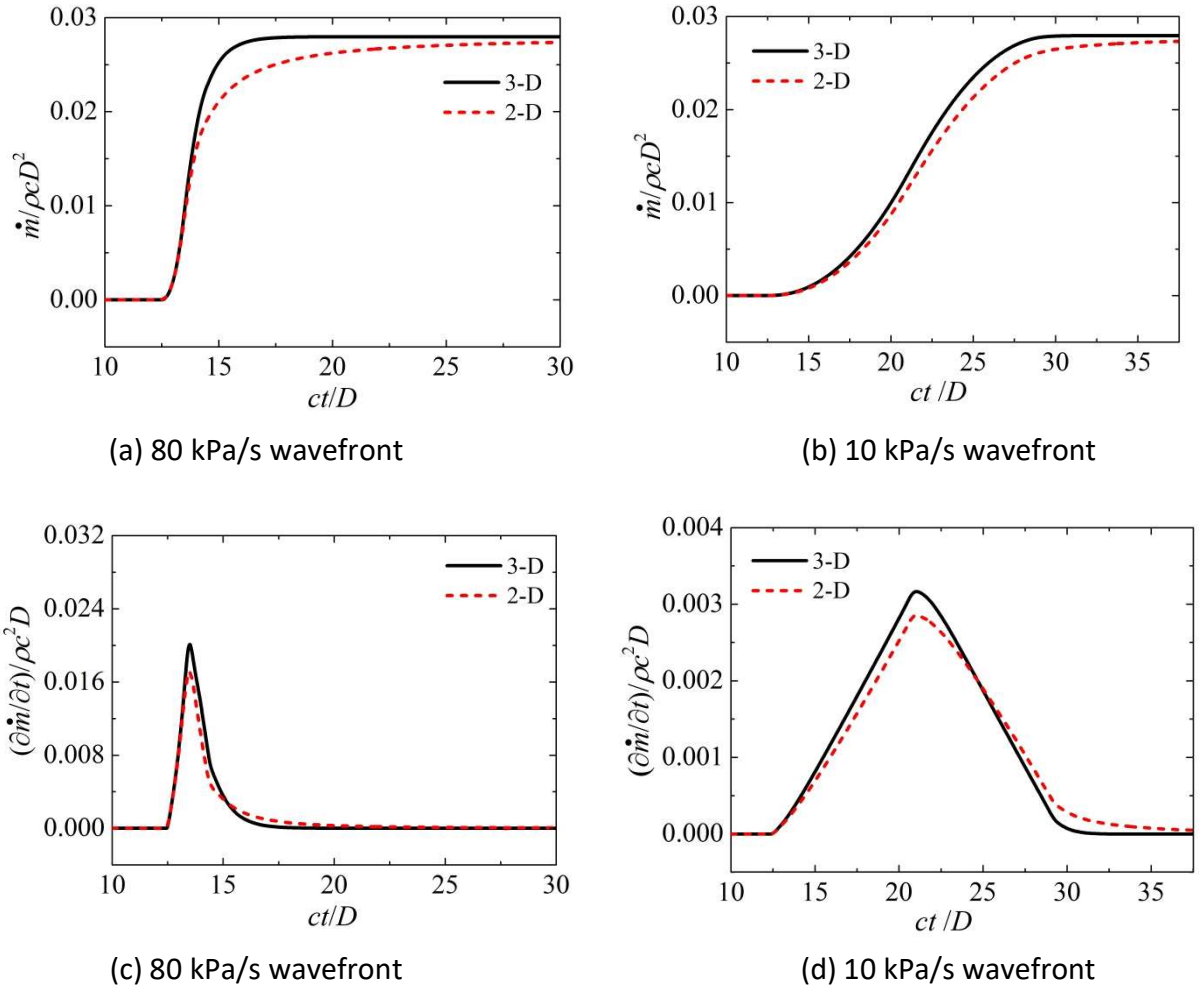

(a) 80 kPa/s wavefront

(b) 10 kPa/s wavefront

(c) 80 kPa/s wavefront

(d) 10 kPa/s wavefront

Fig.6. Flow rates through the portal: absolute values and rates of change (Overground 3-D; Cutting 2-D)

NB: For the 2-D case, $\dot{m}$ should be interpreted as $D\dot{m}_z$

Another feature of the flow rate histories is the ratio of the maximum values for the 2-D and 3-D cases. These are approximately 0.847, 0.855, 0.869 and 0.902 for the 80, 40, 20 & 10 kPa/s wavefronts respectively (although these values are listed to three-digit precision only for qualitative purposes). That is, the maximum flow rates induced in the 2-D case are approximately 10 - 15% smaller than those in the 3-D case. This is consistent with the sustained pressures at the exit in Fig.5. It is intuitively reasonable because of the greater restriction imposed by the smaller volume of the 2-D external domain.

4 RADIATION FROM TUNNEL EXITS

Radiated pressure histories on the x-axis in the 2-D external domain (cutting) are shown in Fig.7 at distances of D, $2D$ and $4D$ from the portal. The ranges of the vertical axes are chosen in

proportion to the *square roots* of the wavefront steepnesses, again giving a simple visual indication of the approximate relative amplitudes of the maximum values. In this case, however, the scaling differs greatly from scales that would be used for radiation from overground portals, where the corresponding dependence is well known to approximate closely to a *linear* dependent on the steepnesses of incident wavefronts. Analytical expressions for both geometries are given in Section 5.

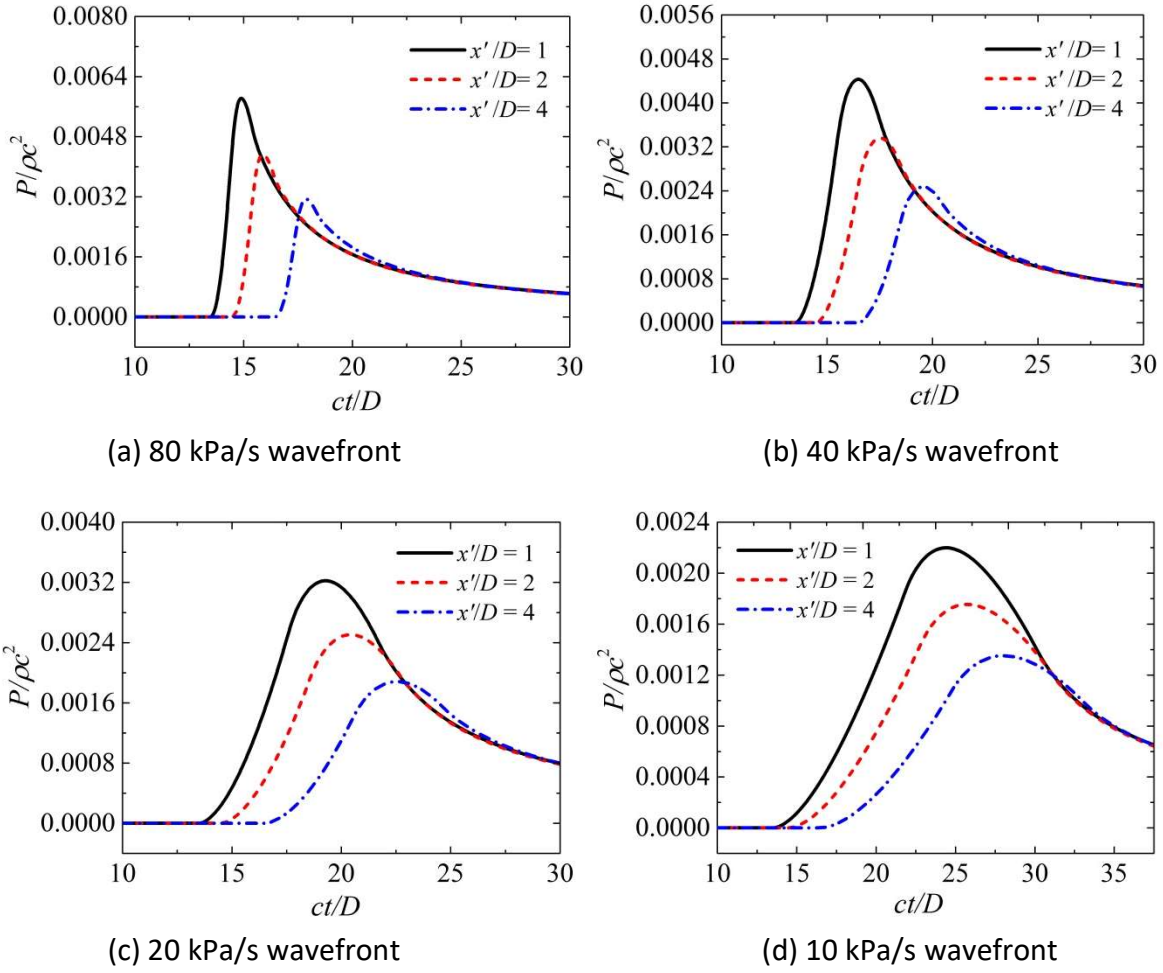

(a) 80 kPa/s wavefront

(b) 40 kPa/s wavefront

(c) 20 kPa/s wavefront

(d) 10 kPa/s wavefront

Fig.7. Radiated pressure histories outside the tunnel: 2-D external geometry

Fig.8 presents the same basic data as Fig.7, but with two adjustments. Firstly, the pressures are expressed as a product with the square root of the distance *r* from an effective focal point upstream of the portal. This is a point from which waves sufficiently far beyond the portal appear to have originated. Herein, its location is inferred by examination of the predicted external pressures, and it is found to be dependent upon the wavefront shape. However, all inferred values are close to a distance of 0.4*D* upstream of the exit plane so, for consistency, this value is used for all comparisons in Fig. 7. With this scaling factor, the maximum amplitudes of the histories at the three distances are almost equal. This shows that the peak values vary approximately with the inverse of the square root of the distance from the focal point. This is

another major difference from the overground case, in which the pressures vary with the inverse of *r*, not with its square root.

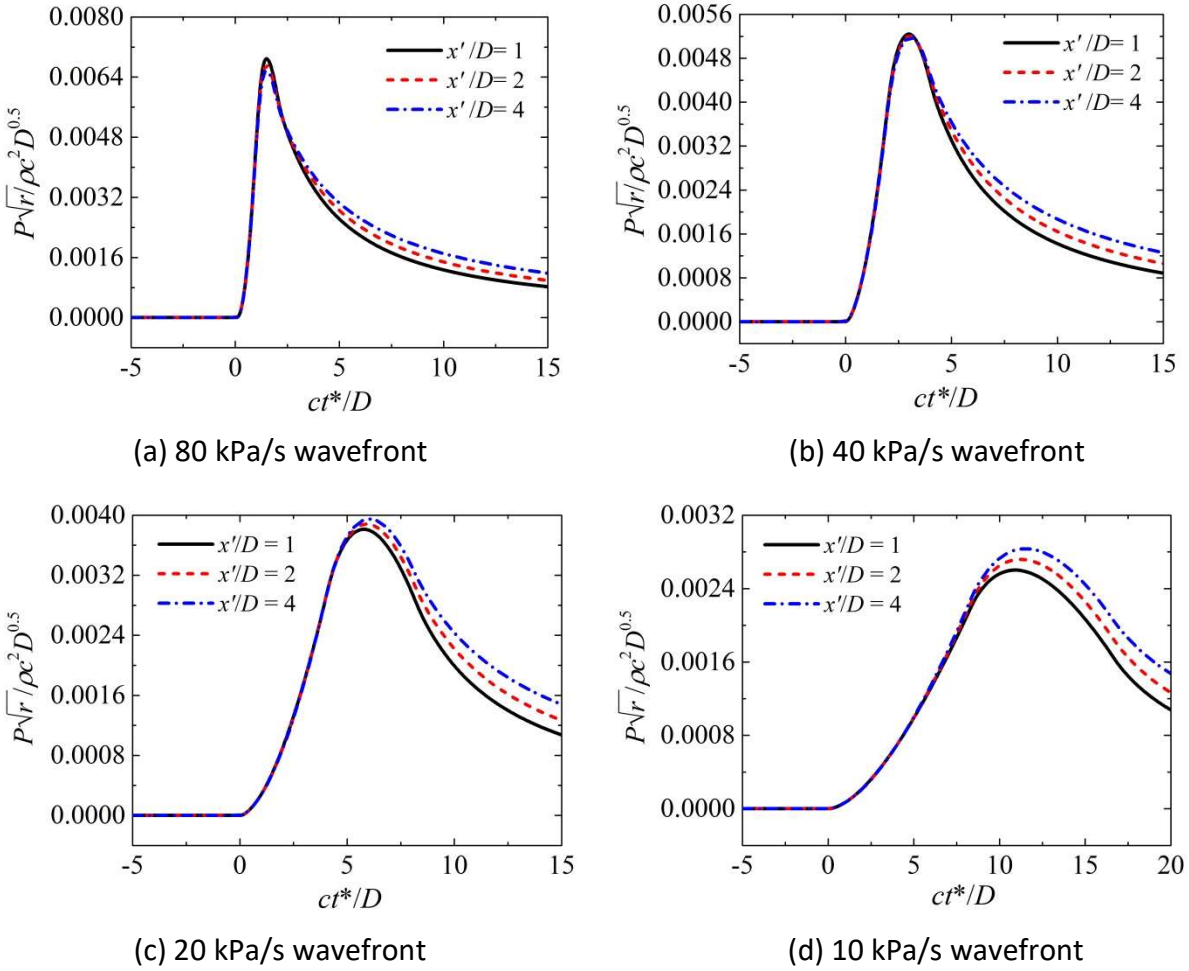

(a) 80 kPa/s wavefront

(b) 40 kPa/s wavefront

(c) 20 kPa/s wavefront

(d) 10 kPa/s wavefront

Fig.8. Weighted pressure histories outside the tunnel: 2-D external geometry

The second adjustment made in the lower row of the figure is a simple time shift that compensates for the time required for the pulse to travel (at the speed of sound) between the various locations. For each graph, the retarded time $t^* = 0$ corresponds to the instant when the leading tip of the wavefront reaches the sampling point, having travelled from the upstream boundary at the ambient speed of sound since the instant $t = 0$. With these adjustments to the pressure and time, it is easily seen that the shapes of the rising limbs of the pulses vary only gently during propagation, but that the falling limbs disperse quite strongly as the pulse propagates. This strong dispersion is consistent with the qualitative behaviour of the corresponding reflected wavefronts and mass flow rates described in the preceding Section. Quantitative use of this similarity is made in Section 5.

The existence of the approximate correlation is not surprising because even closer correlations exist for the overground radiation. Not only do the peak pressures scale very closely with the inverse of the distance *r*, but also the whole pulse scales in this way. That is, the shape of the

whole pulse (falling as well as rising limbs) remains almost exactly constant as it propagates – and, in practice, this makes it possible for the overall propagation to satisfy simple analytical expressions that are used routinely when assessing MPWs. Unfortunately, the dispersive character of the corresponding 2-D pulses precludes such an outcome. However, it is shown below that a simple analogous formula is able to predict the peak pulse amplitudes with sufficient accuracy to be useful during engineering design. As an aside, attention is drawn to an intriguing result presented by Bender et.al.[17], namely that the dispersion can be eliminated by adding a second time dimension.

5 APPROXIMATE EXPRESSION FOR 2-D RADIATION

For overground portals, the pulse radiated from a tunnel can be approximated using simple acoustic formulae that relate the pulse amplitude to the rate of mass flow through the portal at an earlier instant determined by the time required for waves to travel from the portal to the sampling point. The resulting pressures depend upon the overall geometry and the simple formulae apply for two extreme cases. At one extreme, the conditions could resemble those depicted in Fig.1a and, for this case, the radiation approximates quite well to a simple combination of a monopole and a dipole. That is the amplitude p of the pulse at a distance r from the effective source satisfies[18]

Monopole + Dipole:
$$p(r,t^*) = (1+\frac{\ell}{r}\cos\theta)\frac{1}{\Omega r}\left(\frac{\partial \dot{m}}{\partial t}\right)_{source} \quad (5)$$

in which t^* is the retarded time at which the instantaneous rate of change of flow at the source was $\partial\dot{m}/\partial t$. The parameter Ω denotes a solid angle characterising the extent of the domain encompassing the radiation, ℓ is the end correction described in Section-3 and θ is an angle in the x,z plane (zero and π in the positive and negative x-directions and ½π in the z-direction). For an unflanged portal, $\ell \approx 0.31D_{tun}$, where D_{tun} is the diameter of a circle with the same cross-sectional area as the tunnel.

In the particular case of a flanged portal – i.e. the portal of a tunnel emerging at the bottom of a vertical cliff, the dipole term in Eq.5 can be discarded and the pressures is modelled as[19]

Monopole:
$$p(r,t^*) = \frac{1}{\Omega r}\left(\frac{\partial \dot{m}}{\partial t}\right)_{source} \quad (6)$$

Extensive use of this approach has been made in practical assessments of radiation from railway tunnel portals[3,20] even though it is strictly suitable only for a special geometry. Figure 9 shows a comparison between Eq.6 and numerical predictions obtained in the manner described above for a flanged 3-D case. It can be seen that the whole of the pulse, including the falling limb as well as the rising limb, correlates almost exactly with rates of change of mass flow rate through the portal (as assumed in Eq-6). It will be seen later that this contrasts with the corresponding 2-D case for a portal in a cutting. Figure 9 also serves a second useful purpose; it provides a measure of the

accuracy of the CFD methodology used herein. This is strong evidence for present purposes because rates of change in the 3-D are greater than those in the 2-D case and hence are more demanding computationally.

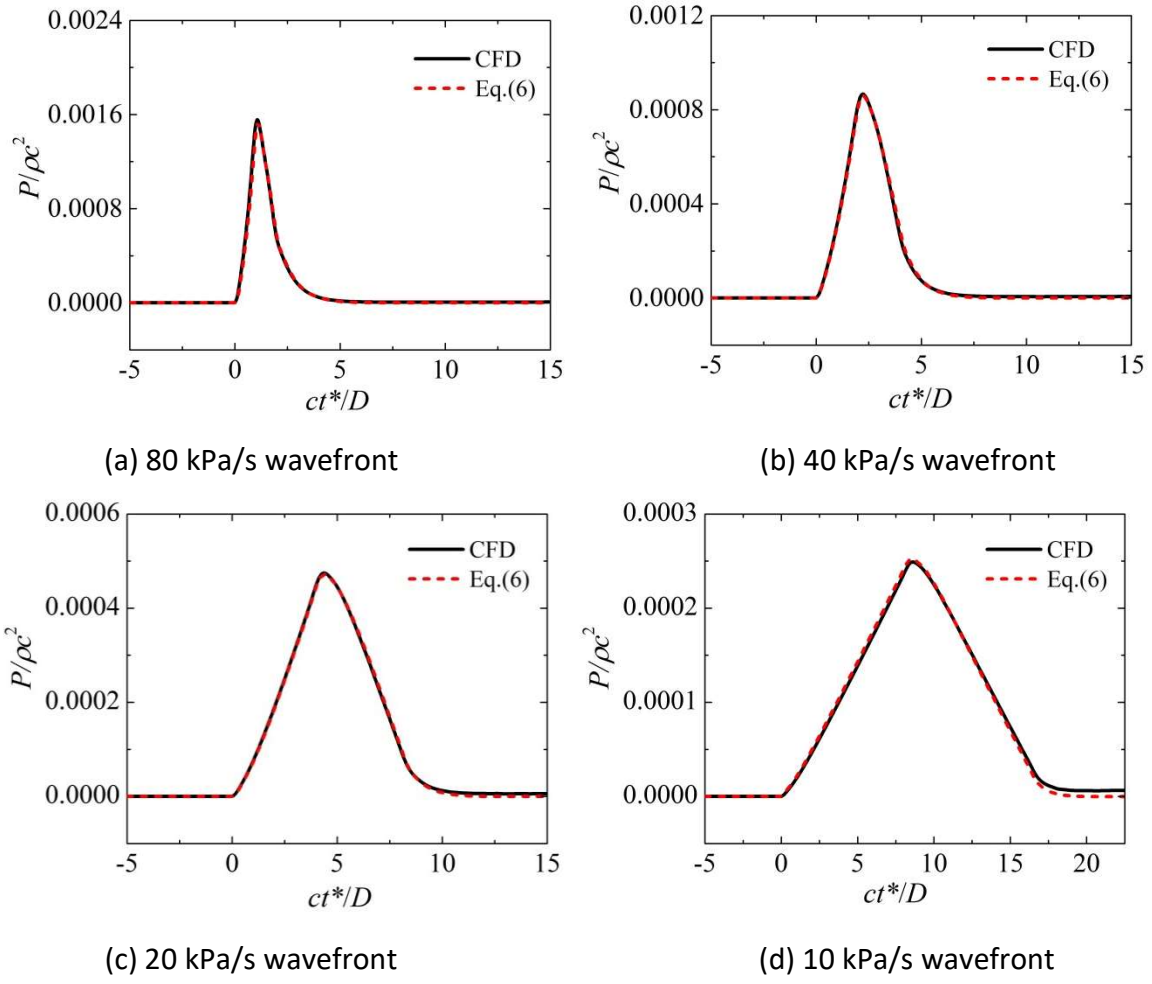

(a) 80 kPa/s wavefront

(b) 40 kPa/s wavefront

(c) 20 kPa/s wavefront

(d) 10 kPa/s wavefront

Fig.9. Comparison of Eq.(6) and CFD predictions at *x*' = 2*D*
(3-D geometry with flanged portal, Ω= 2π)

5.1 2-D domains

Miyachi and Fukuda[18] show that radiation from typical overground portals approximates more closely to the (unflanged) Eq-5 than to (flanged) Eq-6. Nevertheless, the geometry for portals emerging to a deep cutting will usually approximate more closely to the flanged case and so radiation will be nearly independent of direction. That is, just as radiation from a flanged overground portal is approximately spherical, so radiation from a flanged portal in a cutting is approximately cylindrical. Ideally, an expression such as Eq-6 should be developed for this case, but that is not practicable. For example, Lighthill[6] has shown that, at large distances from the source, the behaviour depends on the (½)th derivative of the flow rate history from the source. This is the reason for the continued variation in pressure seen in Fig-6 even after the main pulse has passed. Nevertheless, there is an engineering need for an expression that can be used with

confidence, at least for initial design purposes. Therefore, to simplify matters, a less daunting objective is adopted, namely the development of an approximate method of estimating the most important single property of the pulse - its peak amplitude.

The development of the proposed expression is necessarily empirical, but it is based on two firm observations presented above, namely:

- the peak amplitudes vary approximately with the square root of the maximum flow rate
- the peak amplitudes reduce approximately with the square root of the distance from the effective source

By analogy with Eq-6, these observations suggest that a suitable functional form of the desired expression will be

Functional form:
$$p_{max}(r) \propto \frac{1}{r^{0.5}}\left[\left(\frac{\partial \dot{m}_z}{\partial t}\right)_{max}\right]^{0.5} \tag{7}$$

in which $\partial \dot{m}_z/\partial t$ is the rate of change of mass flow rate per unit width normal to the plane of propagation (i.e. the *z* direction in Fig.3). For this expression to be of practical value, it is necessary to quantify the proportionality. This has been done by means of a detailed assessment of the numerical predictions, interpreted in the non-dimensional manner used above, leading to the following quantitative formula for predicting the peak amplitudes of the pulses:

Peak amplitude:
$$p_{max}(r) \approx \frac{0.053}{r^{0.5}}\left[\left(\frac{\partial \dot{m}_z}{\partial t}\right)_{max}\right]^{0.5} \tag{8}$$

The non-dimensional coefficient 0.053 applies when each of the parameters *p*, *r*, t^* and $\partial \dot{m}_z/\partial t$ is expressed in its non-dimensional form defined in Section 2.3. Alternatively, if a dimensional form is preferred, the coefficient can be replaced by $0.053c(\rho D)^{½}$.

Equation 8 is directly applicable only to the specific geometry under consideration, namely to a flanged portal. This will almost always be the case in a deep cutting, so no attempt has been made to generalise the expression to embrace other geometries in the manner that is done for overground portals and gives rise to the inclusion of the solid angle in Eqs- 5 & 6.

The approximate validity of Eq-8 is illustrated in Fig.10, in which it is compared with values obtained from the CFD analyses. As expected for such a dispersive phenomenon, the correlation is not exact, but it is likely to be adequate for initial design purposes and, perhaps, even for final design when the predicted pulse amplitudes are sufficiently small. In this context, it is useful to bear in mind that it is rare for designers to be able to estimate the portal flow rates with high accuracy. Uncertainties in those estimations will commonly be much greater that the expected uncertainties in Eq-8. An identical difficulty exists when seeking to use Eqs-5 & 6.for overground portals.

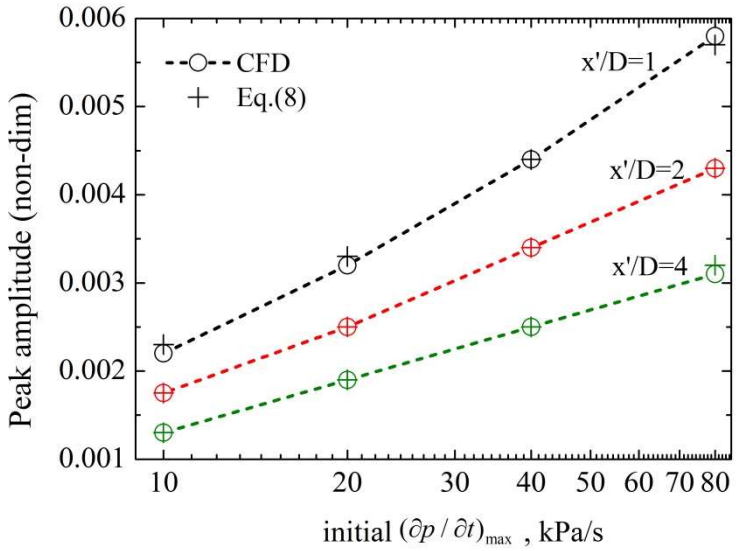

Fig.10 Comparison of the empirical Eq.8 with CFD predictions

Unlike its overground counterparts, Eq-8 applies only to peak values of the pulse pressure and the rate of change of flow through the portal. However, it is instructive to explore a slightly generalised version of the expression, namely:

Indicative equation only:

$$p(r,t^*) = \frac{0.053\left(\frac{\partial \dot{m}_z}{\partial t}\right)}{\left[r\left(\frac{\partial \dot{m}_z}{\partial t}\right)_{max}\right]^{0.5}} \qquad (9)$$

At the peak, this expression is identical to Eq.8, but it also shows the pressures that would exist if the pulse had a one-to-one correspondence with rates of change of flow through the portal. Predictions obtained using this expression are presented in Fig.11. By inspection, it approximately reproduces the rising limbs of the pulses, but not the falling limbs. This is consistent with expectations from Fig-7, but it is more instructive because it shows how strongly the pulses elongate. It is important to emphasize that the authors do not propose the use of Eq.9 in practical applications. Its purpose is simply to assist in the understanding of the physical behaviour of the radiation in the constrained environment of a deep cutting.

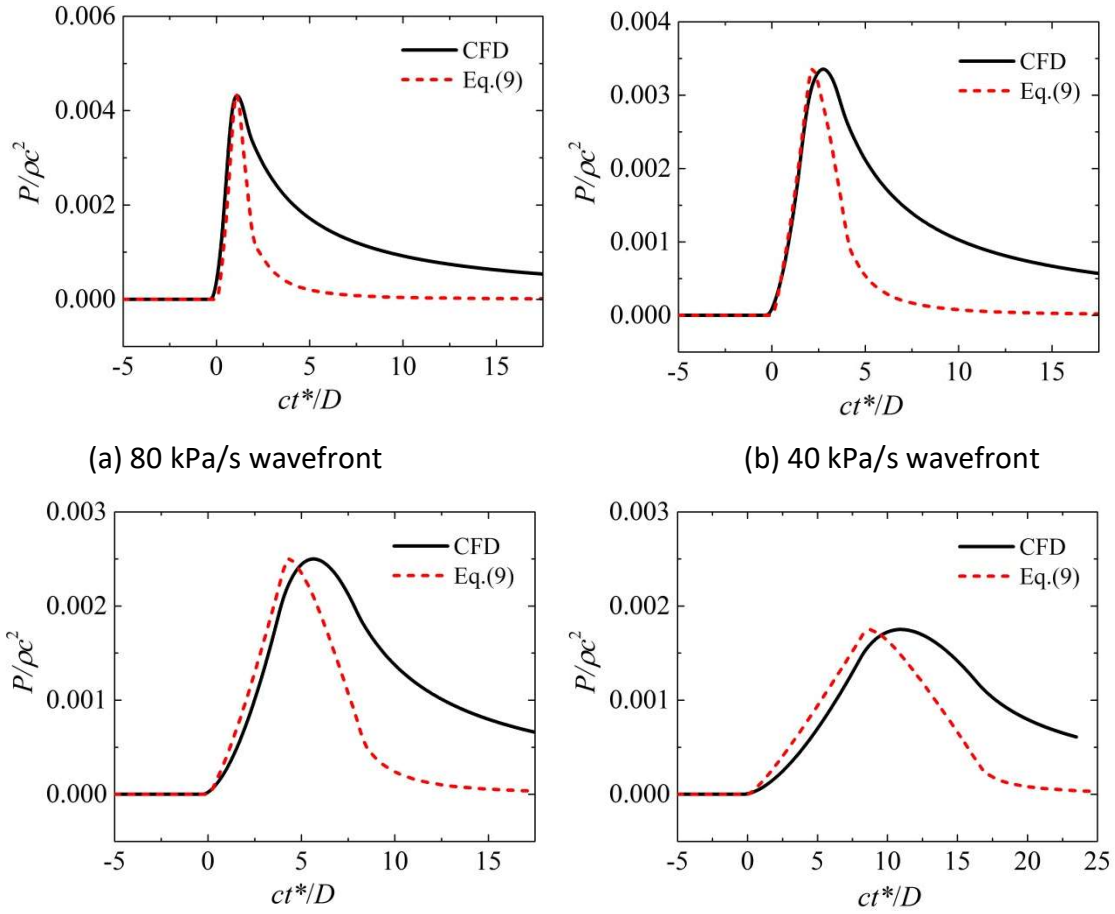

(a) 80 kPa/s wavefront

(b) 40 kPa/s wavefront

(c) 20 kPa/s wavefront

(d) 10 kPa/s wavefront

Fig.11. Comparison of Eq.(9) and CFD predictions at $x' = 2D$

6 IMPLICATIONS FOR IN-TUNNEL PRESSURES AND MICRO-PRESSURE WAVES

The focus of this paper is on understanding large differences between pressure pulses radiated from tunnel portals in deep cuttings and the corresponding pulses from overground portals. However, brief attention is now given to potential practical implications of the outcomes.

Inside tunnels, the increased elongation of wavefronts reflected from portals in cuttings will slightly reduce extreme values of pressure changes in short periods relevant to passenger aural pressure comfort[21] and to sudden forces on train bodies.[14] However, these topics are not likely to be strongly influential in the overall design process, so although the small benefit is likely to be welcome, it will not be decisive.

Outside tunnels, the overriding outcome is a strong increase in pressure amplitudes at any particular distance in comparison with the above-ground case. This has implications for criteria relating to the acceptability of allowing railway staff to operate inside cuttings during train operation. It is also noteworthy, however, that the increased amplitudes are offset to some extent by corresponding reductions in frequency resulting from the strongly-dispersive character

of the radiation. Such reductions will be especially significant when they cause frequencies to fall below the audible range.

All of the results presented herein have been obtained for specific wavefronts that have a simple 'S' shape that is indicative of many pressure waves in railway tunnels. In the case of overground portals, this is not an important limiting factor because the pulse radiation has a one-to-one correspondence with rates of change of flow through the portal. It is already known that Eqs-5 & 6 can be used regardless of the shape of the incident wavefront. Thus, for example, the maximum pulse amplitude will always correspond to the maximum rate of change of flow rate, regardless of the overall shape of a wavefront. However, the same assertion cannot be made with full confidence for portals in deep cuttings, even though it is assumed in Eq-8. This is because dispersion causes the pulse pressure at any particular radius and time to be influenced by portal flows at all times up to the principal retarded time that has sole control in the 3-D case. Nevertheless, the equation has been shown to apply closely even for wavefronts with steepnesses differing by a factor of four, thereby indicating that the dependence on earlier times is relatively weak during the rise time of a rapid pulse. This is the period of greatest significance for design purposes. The influence of dispersion does not become strong until after the peak has been reached.

7 CONCLUSIONS

The reflection of steep wavefronts arriving at a tunnel portal in a deep cutting and the consequential radiation of MPWs beyond the tunnel have been investigated and compared in detail with the corresponding phenomena for portals above ground. The above ground case has been investigated extensive by numerous researchers, but the authors are not aware of any previous study related to wave propagation in cuttings. Indeed, no comparable study related to any other application with similar geometry has been found even though many existing CFD packages are eminently capable of simulating such phenomena. This is assumed to be an indicator that cuttings are a rare instance of practical applications in which wavefront propagation in 2-D geometry is important.

The investigation has been undertaken using commercially-available CFD software that is widely used and the solutions obtained have been shown to exhibit negligible dependence on the chosen numerical grid structure. In addition, previous work has been cited in which predictions of wavefront propagation, including inertial steepening effects, have been validated by comparison with analytical expressions.

It has been shown that the reflection/radiation process for portals in deep cuttings exhibits strong dispersion that is absent in the above-ground case. The dispersion causes long delays in the full development wavefronts reflected back along a tunnel. It has been shown that this behaviour cannot be represented satisfactorily by an existing practice that is sometimes adequate for overground portals, namely imagining that the reflection effectively occurs in a plane a short distance outside the portal.

Corresponding delays in radiation beyond the portals have been shown to have only a weak influence on steep rising limbs of propagating pulses, but a strong influence on their falling limbs. For engineering design purposes, this is a fortuitous result because the rising limbs of the pulses are much more important than the falling limbs. Furthermore, it has made it possible for an approximate analytical equation to be developed and used to predict the maximum amplitudes of pulses emitted into deep cuttings. The equation shows that the maximum amplitude of any particular pulse decays with increasing distance much more slowly that its counterpart for overground portals. In the cutting, the maximum amplitude is approximately proportional to $r^{-0.5}$ whereas, overground, it is approximately proportional to r^{-1}, where r is the distance from the portal.

Another important difference from the overground case is that the new equation for the maximum amplitude of the radiated pulse cannot be generalised to representing the detailed shape of the whole pulse. Its inadequacies during the period of increasing to a maximum are expected to be acceptable in engineering practice, but the same is not true during the subsequent decay that is so strongly influenced by the delays that cause strong dispersion.

The practical significance of the work has been discussed briefly, including drawing attention to some topics that would benefit from further investigation.

FUNDING

This work was supported by the National Natural Science Foundation of China [grant number 51808460 and Sichuan Science and Technology Program [grant number 2021YFG0214].

DECLARATION of CONFLICTING INTERESTS

The Author(s) declare(s) that there is no conflict of interest.

REFERENCES

1. Deeg P, Hieke M, Gerbig C, et al. Micro-pressure wave countermeasures realized in the Katzenberg tunnel and introduction of a new German micro-pressure wave regulation. In: *the 15th international symposium on Aerodynamics, Ventilation and Fire in Tunnels*, Barcelona, Spain, 18-20 September 2013, BHR Group, pp. 577-588.
2. Miyachi T. Acoustic model of micro-pressure wave emission from a high-speed train tunnel. *J Sound Vib* 2017; 391:127–152.
3. Ozawa S, Maeda T, Matsumura T, et al. Micro-pressure waves radiating from exits of Shinkansen tunnels. *QR OF RTRI* 1993; 34 (2):134–140.
4. Wang HL, Vardy AE and Bi HQ. Micro-pressure waves from tunnel portals in cuttings. In: *the 18th international symposium on Aerodynamics, Ventilation and Fire in Tunnels*, Greece, 25-27 September 2019, BHR Group, pp. 206-220.
5. Balazs NL. Wave propagation in even and odd dimensional spaces. *Proc Phys Soc A 1955; 68:521-523.*
6. Lighthill MJ. *Waves in Fluids*. Cambridge: Cambridge University Press, 1978.

7. Beranek LL, Mellow TJ. The wave equation and solutions. In: Beranek LL and Mellow TJ (eds) *Acoustics: Sound Fields and Transducers*. Academic Press, 2012, pp.21-63.
8. Anco SC, Ivanova NM. Conservation laws and symmetries of semilinear radial wave equations. *J Math Ana Appl* 2007; 332: 863–876.
9. Kluwick A. The analytical method of characteristics. *Prog Aerospace Sci 1981; 19:197-313*
10. Williams GE. Cylindrical Waves. In: *Fourier Acoustics-Sound Radiation and Nearfield Acoustical Holography*. Academic press, 1999, pp.183-234.
11. ANSYS FLUENT User Manual, Release 15.0,2014.
12. Wang HL, Vardy AE and Pokrajac D. Perforated exit regions for the reduction of micro-pressure waves from tunnels. *J Wind Eng Ind Aerodyn* 2015; 146: 139–149.
13. UIC, 2018. Railway Applications – Aerodynamics – Part 5: Requirements and test procedures for aerodynamics in tunnels. European Standard EN 14067-5(provisional regulation).
14. Sima M, Schulz B, Gölz P, et al. Dynamic pressure tightness of very high-speed train CRH380D. *In: the 16th international symposium on Aerodynamics, Ventilation and Fire in Tunnels*, Seattle, USA, 15-17 September 2015, BHR Group, pp.467-481.
15. Rienstra SW, Hirschberg A. *An Introduction to Acoustics*. Extended and revised edition of IWDE 92-06. Eindhoven: Eindhoven University of Technology, 2004. http://www.win.tue.nl/~sjoerdr/papers/boek.pdf
16. Duan W, Kirby R. A hybrid finite element approach to modeling sound radiation from circular and rectangular ducts. *J Acoust Soc Am* 2012; 131 (5):3638 -3649.
17. Bender CM, Rodriguez FJ, Sarkar S, et al. Two-dimensional wave propagation without anomalous dispersion. *Phys Rev Lett* 2017; 119: 114301.
18. Miyachi T, Fukuda T. Experimental Investigation of the Effects of Topography Around the Tunnel portal on Micro-pressure Waves. *QR OF RTRI* 2014; 55(4): 235-240.
19. Blake WK. *Mechanics of flow-induced sound and vibration*. Academic Press, Orlando Vol.1, 1986.
20. Zhang G, Kim TH, Kim DH, et al. Prediction of micro-pressure waves generated at the exit of a model train tunnel. *J Wind Eng Ind Aerod* 2018; 183:127–139.
21. Claus P, Deeg P, Tielkes T. A new approach to assess aural pressure comfort in high-speed trains running on German high-speed lines with single-track tunnels. *In: the 17th international symposium on Aerodynamics, Ventilation and Fire in Tunnels*, Lyon, France, 13-15 September 2017, pp.71-77.

APPENDIX NUMERICAL ACCURACY

Comparisons presented in Section 5 demonstrate that the numerical analysis is sufficiently accurate for only very small differences from the monopole behaviour to be detectable. Nevertheless, it is useful to demonstrate formally that the chosen grid size is sufficiently small to have negligible influence on the predictions. For this purpose, comparisons are focussed on a location where the strongest spatial changes exist, namely the 90° corner between the tunnel ceiling and the vertical face of the cutting in the plane of the portal (i.e. at $x = L$ and $y = D/2$ – see Fig.3). Likewise, the comparisons are presented for the case that causes the strongest temporal changes, namely the steepest wavefront and the 3-D external environment.

Fig.12 shows predicted instantaneous pressures parallel and normal to the axis for the 3-D geometry when the toe of the steepest wavefront has travelled a distance 2*D* beyond the exit plane. Both lines pass through the point {*L*, *D*/2, 0}. The line parallel to the *x*-axis is on the tunnel ceiling when *x*/*D* < 12.5 and beyond the tunnel when *x*/*D* > 12.5. The line parallel to the *y*-axis is in the portal plane when *y* < *D*/2 and on the vertical face above the portal when *y* > *D*/2. Predictions are shown for two grid sizes, namely Δ*x*/*D* = 1/20 and 1/40. Except close to the corner the differences between the two in the external domain are negligible, but small differences are seen close to the corner. This region is shown at a larger scale in the figures, using discrete points to indicate the grid spacing. This shows that the differences in the smaller scale graphs are attributable in part (although only in part) to the influence of discretisation. In the main body of the paper, a grid size of Δ*x*/*D* = 1/40 has been used for calculations with the 80 kPa/s wavefront, but a grid size of Δ*x*/*D* = 1/20 has been used for the other two wavefronts, for which all changes are less rapid.

For completeness, it is noted that the small differences between the predictions with the two grid sizes include any inaccuracies in the prediction of wavefront steepening along the tunnel as well as inaccuracies introduced at the corner itself. That is, the strong level of agreement has the supplementary effect of demonstrating that numerical dispersion during propagation along the tunnel is small in comparison with the wavefront steepening process. This can be interpreted as confirmation that the time steps used in the calculations are suitable. These satisfy $c\Delta t/\Delta x = 0.30$, which has previously been shown by Wang et al [4,7] to be optimum for simulating wavefront steepening in a tunnel – even though the optimum value of this ratio for explicit 1-D simulations is close to unity.

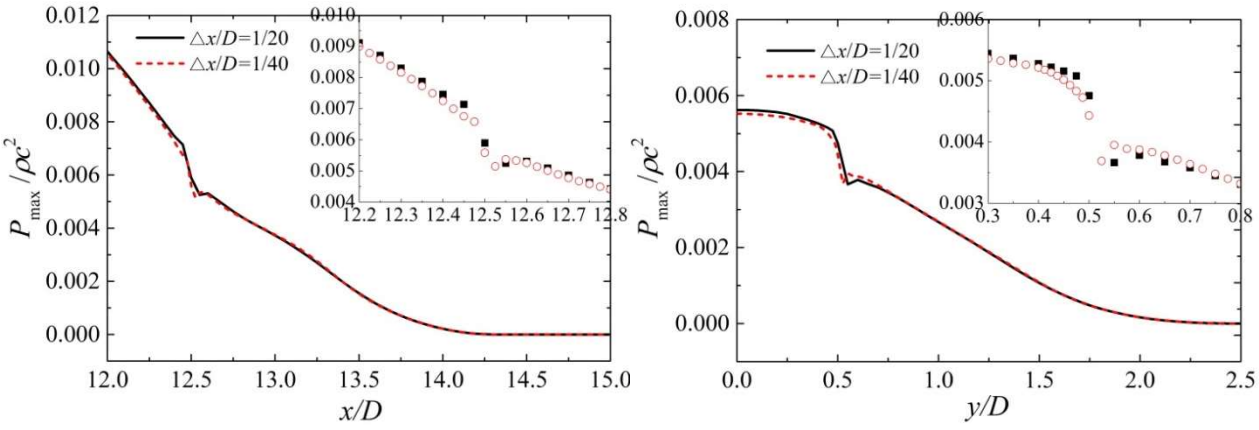

(a) Along *y* = *D*/2, *z* = 0 (b) Along *x* = *L*, *z* = 0

Fig.12. Grid-size dependence close to a 90° corner between the tunnel and the vertical wall (80 kPa/s wavefront, 3-D external geometry)